PCCP

COMMUNICATION

View Article Online
View Journal

Cite this: DOI: 10.1039/c5cp07580g

Received 8th December 2015,
Accepted 23rd January 2016

DOI: 10.1039/c5cp07580g

www.rsc.org/pccp

Equation of state for water and its line of density maxima down to −120 MPa†

Gaël Pallares,[a] Miguel A. Gonzalez,‡[b] Jose Luis F. Abascal,[b] Chantal Valeriani[b] and Frédéric Caupin*[a]

As water is involved in countless natural and industrial processes, its thermodynamic properties have been measured in a wide temperature and pressure range. Data on supercooled water are also available down to −73 °C and up to 400 MPa. In contrast, data at negative pressures are extremely scarce. Here we provide an experimental equation of state for water down to −120 MPa. In particular, we obtain the line of density maxima (LDM) of water down to a pressure six times more negative than previously available. As temperature increases from 4 up to 18 °C, the pressure $P_{LDM}(T)$ along the LDM decreases monotonically from 0 down to −120 MPa, while the slope dP_{LDM}/dT becomes more negative. The experimental results are compared with molecular dynamic simulations of TIP4P/2005 water and a two-state model. We also discuss the possibility to observe extrema in compressibility and heat capacity at negative pressures, features that have remained elusive at positive pressures.

Liquid water can exist below the melting point of ice, in a metastable, supercooled state. Supercooled water exhibits numerous thermodynamic and dynamic anomalies,[1,2] involved in phenomena such as crystallization and vitrification both of water and of aqueous solutions.[3] Several scenarios have been proposed so far to explain the origin of water anomalies,[4–6] but experiments have not yet allowed to select the most convincing one. When water is stretched at a density lower than the stable liquid, it becomes metastable with respect to the vapor phase and its pressure may even become negative. Negative pressures are possible because of cohesion between water molecules.[7] They are used by trees to pull sap up to their top,[8] and thought to be relevant for water confined in nanopores.[9]

The most famous anomaly of water is arguably its density maximum near 4 °C at ambient pressure, a macroscopic manifestation of hydrogen bonding. The temperature T at which the maximum occurs as a function of pressure P defines the line of density maxima (LDM). The LDM has been measured far in the supercooled liquid at 120 MPa down to around −40 °C,[10] but only at moderate negative pressure, the current record being −20.3 MPa at 7.7 °C.[11] In this pressure range, the slope dP/dT of the LDM is negative. Theoretical scenarios proposed to explain water anomalies give conflicting predictions for the shape of the LDM at a larger negative pressure: it might maintain a negative slope,[4,12] or reach a turning point.[5,6] Previous measurements of the LDM in stretched water were limited to −20 MPa because of nucleation of the vapor phase. There is only one experimental method at present that is able to significantly exceed this limit:[13] the microscopic Berthelot tube (MBT).[14–17] However, previous MBT studies estimated the negative pressure from the extrapolations of positive pressure data. In this work we analyse sound velocity data at $P < 0$ generated by the MBT method[18] to obtain an experimental equation of state (EoS) for water down to −15 °C and −120 MPa. This exceeds by far any previous study (such as one that reached −26 MPa at ambient temperature[19]), allowing a direct calibration of the pressure in the MBT method to determine the LDM down to −120 MPa.

Another relevant issue one should consider is the fate of the isothermal compressibility κ_T in supercooled water, since it may diverge[1,4] or go through a maximum.[6,20,21] Numerous experiments have addressed this question (see ref. 2 for a review), but crystallization (which irremediably occurs at around −40 °C) always prevented reaching a definite answer. In this report, we consider whether applying negative pressure may allow the observation of extrema in κ_T along isobars.

In our experiments, negative pressures are generated by means of an MBT.[14–17] Micrometer-sized inclusions in a quartz

[a] Institut Lumière Matière, UMR5306 Université Claude Bernard Lyon 1-CNRS, Université de Lyon and Institut Universitaire de France, 69622 Villeurbanne cedex, France. E-mail: frederic.caupin@univ-lyon1.fr

[b] Departamento de Quimica Fisica I, Facultad de Ciencias Quimicas, Universidad Complutense, 28040 Madrid, Spain

† Electronic supplementary information (ESI) available: Materials and methods, choice of the interpolating function for sound velocity data, construction of an equation of state from sound velocity data along isochores, correction due to quartz compliance, propagation of errors, results and sensitivity to the interpolation function, and details about the two-state model for water and about the calculations of the lines of density maxima from numerical simulations of TIP4P/2005. See DOI: 10.1039/c5cp07580g

‡ Current address: Department of Chemistry, Imperial College London, SW7 2AZ, London, UK.

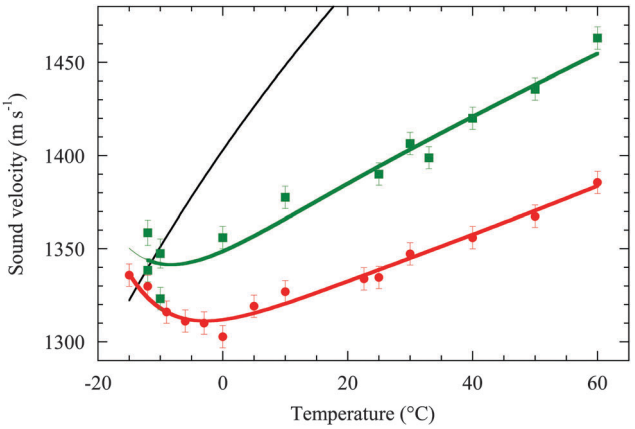

Fig. 1 Sound velocity c in stretched water. $c(T)$ is shown along the isochore at ρ = 1000 kg m^{-3} (black curve), and for sample 1 (red discs) and 2 (green squares) with nominal densities ρ_1 = 933.3 ± 0.5 kg m^{-3} and ρ_2 = 951.9 ± 0.6 kg m^{-3}, respectively.[18] To generate an EoS, the data are interpolated with simple functions (red and green curves) (see the ESI†). The thinner section of the green curve below −12 °C shows the region involving an extrapolation of the sample 2 data.

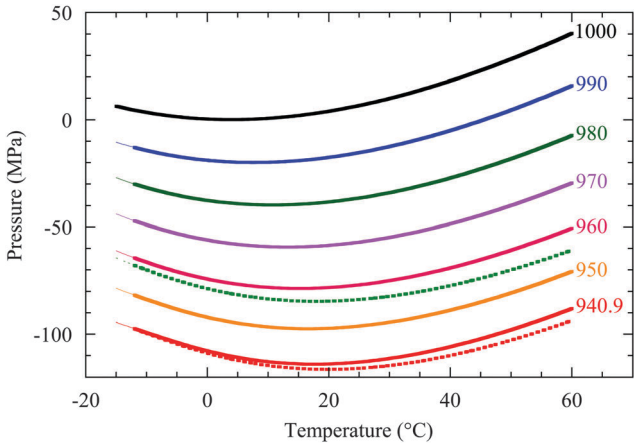

Fig. 2 Pressures along several isochores. Different curves correspond to different densities (in kg m^{-3}). Their thinner sections (at low temperatures) show the region which is based on the sample 1 data only, involving an extrapolation of the sample 2 data. The actual pressure in the samples (dotted lines) deviates slightly from an isochore because of the compliance of the quartz matrix (see the ESI†).

crystal are filled with liquid water, and cooled at a nearly constant volume. When negative pressure develops, a vapor bubble usually appears in the liquid, destroying the metastability. However, careful choice of the sample and of the density of water allows to avoid cavitation, and to cool the liquid below the temperature of liquid–ice equilibrium. Liquid water is then doubly metastable, with respect to both vapor and ice. We measured the sound velocity in two such samples with Brillouin light scattering[18] (Fig. 1). A minimum was observed at around 0 °C for the lowest density sample. We have adopted state-of-the-art techniques used in condensed matter[22,23] to generate an EoS at negative pressure (see the ESI†). To start with, our sound velocity (c) data are interpolated over the whole temperature (T) and density (ρ) ranges (Fig. 1). The interpolating function is

$$c_{\rm int}(T,\rho) = c(T,\rho_0) + \left(\frac{\partial c}{\partial \rho}\right)_T (T,\rho_0)(\rho-\rho_0) + a_2(T)(\rho-\rho_0)^2 + a_3(T)(\rho-\rho_0)^3, \quad (1)$$

where a_2 and a_3 are functions of the temperature to be determined. We start with a reference isochore at ρ_0 = 1000 kg m^{-3} on which water properties are determined accurately through a multi-parameter equation of state, the IAPWS EoS.[24] This accurate EoS allows us to impose the known values of $c(T,\rho_0)$ and $(\partial c/\partial\rho)_T(T,\rho_0)$. At a given temperature T, there is a unique pair of values (a_2, a_3) for which eqn (1) reproduces the values of $c(T,\rho_1)$ and $c(T,\rho_2)$ taken from the two samples. We first compute this solution for (a_2, a_3) at each temperature for which data are available for sample 2, using the corresponding data for sample 1 (or a linear interpolation between the neighboring data points for −10 and 33 °C). The result is shown in Fig. S1 (ESI†), with the error bars deduced from the experimental uncertainty on the sound velocity. Parameters a_2 and a_3 exhibit a smooth temperature variation, and their ratio (Fig. S1, ESI,† lower panel) is remarkably constant. These observations suggest to use simple interpolating functions for the whole set of $c(T, \rho)$ data. We have investigated 10 possible choices for $a_2(T)$ and $a_3(T)$, listed in Table S2 (ESI†). The quality of the fits and their residuals are discussed in the ESI† (see in particular Fig. S2, S3 and Table S2). In the following, we present results obtained with our best interpolation (number 10 in the ESI†). We also discuss the sensitivity of the procedure to the choice of interpolation. For a given interpolation $c_{\rm int}(T,\rho)$, starting from the knowledge of P and C_P at ρ_0, the integration of thermodynamic relations (see the ESI†) yields P, κ_T and C_P in the whole covered $T-\rho$ range. A small correction for the compliance of the quartz matrix is also included (see the ESI†).

Fig. 2 shows $P(T)$ for a series of isochores. The density at rounded values of temperature and pressure is given in Table 1 for future reference. The minima of the isochores define the location of the LDM, shown in Fig. 3. Table 2 provides temperature and density along the LDM for a series of pressures. Having checked the effect of the uncertainty on the sound velocity and of

Table 1 Density ρ (in kg m^{-3}) at the corresponding temperature and pressure. Only pressures above those reached in sample 1 are given

Pressure/ MPa	Temperature/°C								
	−15	−10	0	10	20	30	40	50	60
0	996.2	998.1	999.8	999.7	998.2	995.6	992.2	988.0	983.2
−10	990.3	992.4	994.6	994.8	993.5	991.1	987.8	983.6	978.8
−20	984.3	986.7	989.4	989.9	988.8	986.5	983.3	979.2	974.3
−30	978.2	981.0	984.1	984.9	984.0	981.9	978.7	974.6	969.8
−40	972.3	975.2	978.7	979.8	979.2	977.2	974.0	970.0	965.1
−50	966.4	969.4	973.3	974.7	974.3	972.3	969.3	965.2	960.3
−60	960.6	963.7	967.8	969.5	969.3	967.5	964.4	960.4	955.4
−70	954.9	957.9	962.3	964.3	964.2	962.5	959.5	955.4	950.4
−80	949.2	952.2	956.8	959.0	959.1	957.5	954.5	950.4	945.2
−90	943.5	946.4	951.2	953.6	953.8	952.3	949.4	945.2	939.8
−100			945.5	948.1	948.5	947.1	944.1	939.8	
−110				942.5	943.1	941.7			

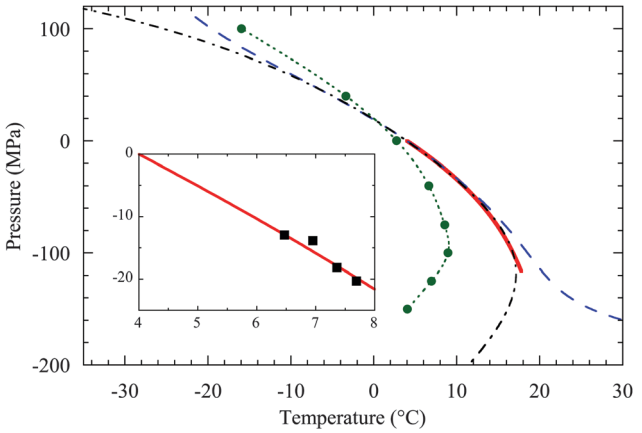

Fig. 3 LDM for water at negative pressures. The present experimental LDM (solid red curve) agrees with the previous determination[11] (inset, filled black squares), and also with the IAPWS extrapolation down to −50 MPa (dashed blue curve), but departs from the latter at larger negative pressures. MD simulations with the TIP4P/2005 potential (green circles and dotted curve) and the extrapolation of the HA model (dash-dotted black curve) are also shown.

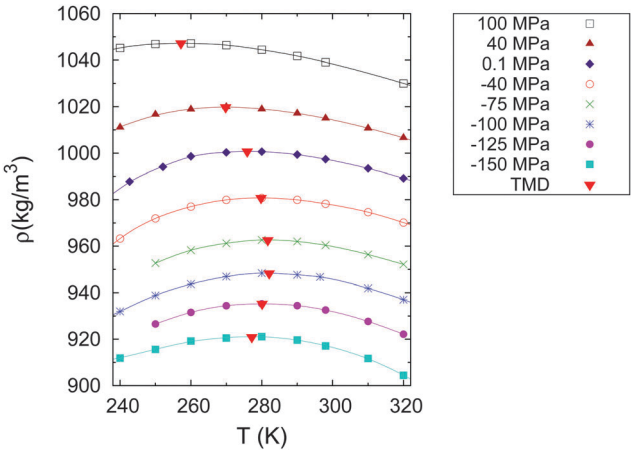

Fig. 4 Simulated isobars for the TIP4P/2005 model. The LDM temperature is indicated by filled red triangles.

the choice of the interpolating function, we conclude that they affect the LDM temperature by at most 0.06 and 0.6 °C, respectively (Fig. S5 and S6, ESI†). Our result is in perfect agreement with a previous determination of the LDM at $P < 0$[11] (Fig. 3, inset), but now the pressure range extends by a factor of six. The only other existing data on the LDM at these extreme negative pressures were indirect, based on the statistics of vapor nucleation in another water inclusion in quartz.[17] This single data point, which has non-negligible error bars, is compatible with our accurate data.

We now compare our experimental results with the extrapolation of the current formulation for the properties of water at $P > 0$[24,25] (IAPWS extrapolation) (Fig. 3). The LDM of the IAPWS extrapolation, based on positive pressure data only, agrees with our data down to −50 MPa, but then bends to higher temperatures and its curvature changes sign. Next we compare with the LDM estimated by means of molecular dynamics (MD). To perform these simulations, we have used the TIP4P/2005 water potential,[26] currently considered to give the best agreement with the experimental properties of water at $P > 0$.[27] Besides, the model fairly compares with the scarce experimental results in the supercooled[28] and doubly metastable regions.[18] Thus, we calculated the LDM with TIP4P/2005 to complement the existing simulations[29] (see the ESI† for details). To do so, we calculated the density at several temperatures along the isobars (results are given in Table S6, ESI†) and located the temperature at which the maximum density is reached (Fig. 4). The numerical result for the LDM is in reasonable agreement with the experimental one (Fig. 3), taking into account that the TIP4P/2005 potential has been fitted on positive pressure data. The slope of the LDM curve appears to be more negative in the MD simulations, but the curvature increases in the same pressure range. However, in a different manner from that of the experiments, the TIP4P/2005 LDM reaches a turning point at a pressure close to the limit of our experiment. To conclude, we compare our experimental results with a thermodynamic model recently developed by Holten and Anisimov (HA model).[30] The HA model assumes that water is an athermal solution of two species with different entropies and densities, which exhibit a transition between two liquids at low temperatures. The transition ends at a liquid–liquid critical point (LLCP). We have calculated water properties at negative pressures based on the mean field version of the HA model. It should be kept in mind that, as simple functional forms were chosen to fit the pressure dependencies of the positive pressure data, the HA model does not include a liquid–vapor spinodal. Yet its extrapolation is well behaved down to large negative pressures, and a comparison with experiments may be attempted. Fig. 3 shows a perfect agreement of the HA model with our experimental LDM. The HA LDM exhibits a turning point at 17.15 °C and −118 MPa, near the turning point of the TIP4P/2005 LDM, and just at the edge of our experimental range.

Next we consider the behavior of the experimental values of κ_T and C_P at a low temperature. At $P > 0$, κ_T and C_P increase monotonically upon cooling at a constant pressure, and upon lowering the pressure at constant temperature, respectively.[2] At $P < 0$, for our best interpolation of the sound velocity data

Table 2 Temperature and density along the LDM at the corresponding pressure

Pressure/MPa	Temperature/°C	Density/kg m^{-3}
0	4.0	999.9
−10	5.9	995.0
−20	7.7	989.9
−30	9.4	984.9
−40	10.8	979.9
−50	12.1	974.8
−60	13.3	969.6
−70	14.4	964.5
−80	15.3	959.3
−90	16.1	954.0
−100	16.8	948.6
−110	17.4	943.1
−116	17.8	939.6

(as measured by its χ^2, see the ESI†), we observe weak maxima, which appear below −50 MPa for κ_T, and below −10.5 °C for C_P (ESI†, Fig. S6). However, using another interpolation with a larger but still acceptable χ^2, these extrema disappear (ESI†, Fig. S6). Therefore, it is not clear if, as suggested by our best interpolation, the minimum in sound velocity measured for sample 1 along a quasi-isochore (see Fig. 1) translates into a maximum in κ_T along an isobar. Being related through $\kappa_T = \gamma c^2/\rho$ with $\gamma = C_P/C_V$, the ratio of isobaric and isochoric heat capacities, it might be that the minimum in sound velocity is compensated by the increase in γ upon cooling. We also note that the two interpolations discussed above differ qualitatively: for our best interpolation, the sound velocity along the quasi-isochore corresponding to sample 2 shows a minimum (Fig. 1), whereas it does not for the other interpolation (see the ESI,† Fig. S2). Therefore, additional data in the doubly metastable region would certainly help establishing the existence or absence of the thermodynamic extrema.

The negative pressure region of the phase diagram appears to be a promising area where decisive experiments can be performed. The shape of the LDM is related to the slope of the liquid–vapor spinodal in the $P-T$ plane.[4] On the one hand, if the LDM maintains a negative slope and intersects the spinodal, the latter reaches a minimum pressure at the junction. On the other hand, if the LDM reaches a maximum temperature and retraces at lower pressures, avoiding the spinodal, the latter maintains a pressure that decreases with decreasing temperature. It would thus be very interesting to measure the LDM at even more negative pressure, to see if a turning point is reached or not. This would require water inclusions with lower densities. However, it is known[14,16,17] that for water density below 910 kg m^{-3}, cavitation occurs above 40 °C, thus preventing access to the LDM. Yet the small interval between 910 and 930 kg m^{-3} deserves further investigation. To elucidate the existence or nonexistence of maxima in κ_T and C_P, more experiments are needed. The present technique, based on Brillouin light scattering, is limited because of low-temperature broadening of the spectra. To access lower temperatures, an improved signal-to-noise ratio is needed, or another technique. One possibility would be to use transient grating experiments.[31] However, they would require larger samples to accommodate the size of the transient grating. Another possibility with our typical fluid inclusions would be to study aqueous NaCl solutions. Indeed, MD simulations predict that the LLCP shifts to a higher temperature and lower pressure with increasing NaCl concentration.[32] To generate negative pressures, other techniques than fluid inclusions in quartz are also available. However, to the best of our knowledge, they do not allow to reach beyond −30 MPa.[13] To be accessible to experiments, the putative κ_T maxima must lie above the line of homogeneous nucleation of ice. Experiments under a positive pressure did not find any sign of maxima in κ_T or C_P before the occurrence of crystallization. As explained in ref. 18, the line of κ_T maxima, if it exists, would reach higher temperatures at negative pressures, and might thus become accessible to experiments.

Acknowledgements

The team at Lyon acknowledges funding by the ERC under the European Community's FP7 grant agreement 240113, and by the Agence Nationale de la Recherche ANR grant 09-BLAN-0404-01. C. V. acknowledges financial support from a Marie Curie Integration Grant 322326-COSAAC-FP7-PEOPLE-CIG-2012 and thanks the Ministerio de Educacion y Ciencia and the Universidad Complutense de Madrid for a Ramon y Cajal tenure track. The team at Madrid acknowledges funding from the MCINNC Grant FIS2013-43209-P and from the UCM/Santander Grupos Complutense 910570, and the computer time allocated in the RES Spanish Supercomputer facility Minotauro (grant numbers QCM-2014-1-0038 and QCM-2014-2-0028).

References

1 R. J. Speedy and C. A. Angell, *J. Chem. Phys.*, 1976, **65**, 851–858.
2 V. Holten, C. E. Bertrand, M. A. Anisimov and J. V. Sengers, *J. Chem. Phys.*, 2012, **136**, 094507.
3 G. Bullock and V. Molinero, *Faraday Discuss.*, 2013, **167**, 371.
4 R. J. Speedy, *J. Phys. Chem.*, 1982, **86**, 982–991.
5 P. H. Poole, F. Sciortino, U. Essmann and H. E. Stanley, *Nature*, 1992, **360**, 324–328.
6 S. Sastry, P. G. Debenedetti, F. Sciortino and H. E. Stanley, *Phys. Rev. E*, 1996, **53**, 6144–6154.
7 F. Caupin and A. D. Stroock, in *Liquid polymorphism*, ed. H. E. Stanley and S. Rice, Wiley, New York, 2013.
8 M. T. Tyree and M. H. Zimmermann, *Xylem Structure and the Ascent of Sap*, Springer-Verlag, Berlin, Heidelberg, New-York, 2nd edn, 2002.
9 A. K. Soper, *Chem. Phys. Lett.*, 2013, **590**, 1–15.
10 O. Mishima, *J. Chem. Phys.*, 2010, **133**, 144503.
11 S. J. Henderson and R. J. Speedy, *J. Phys. Chem.*, 1987, **91**, 3062–3068.
12 S. Sastry, F. Sciortino and H. E. Stanley, *J. Chem. Phys.*, 1993, **98**, 9863.
13 F. Caupin, *J. Non-Cryst. Solids*, 2015, **407**, 441–448.
14 Q. Zheng, D. J. Durben, G. H. Wolf and C. A. Angell, *Science*, 1991, **254**, 829–832.
15 A. D. Alvarenga, M. Grimsditch and R. J. Bodnar, *J. Chem. Phys.*, 1993, **98**, 8392–8396.
16 K. I. Shmulovich, L. Mercury, R. Thiéry, C. Ramboz and M. El Mekki, *Geochim. Cosmochim. Acta*, 2009, **73**, 2457–2470.
17 M. E. M. Azouzi, C. Ramboz, J.-F. Lenain and F. Caupin, *Nat. Phys.*, 2012, **9**, 38–41.
18 G. Pallares, M. E. M. Azouzi, M. A. González, J. L. Aragones, J. L. F. Abascal, C. Valeriani and F. Caupin, *Proc. Natl. Acad. Sci. U. S. A.*, 2014, **111**, 7936–7941.
19 K. Davitt, E. Rolley, F. Caupin, A. Arvengas and S. Balibar, *J. Chem. Phys.*, 2010, **133**, 174507.
20 F. Sciortino, P. H. Poole, U. Essmann and H. E. Stanley, *Phys. Rev. E*, 1997, **55**, 727–737.
21 P. H. Poole, I. Saika-Voivod and F. Sciortino, *J. Phys.: Condens. Matter*, 2005, **17**, L431–L437.

22 L. A. Davis, *J. Chem. Phys.*, 1967, **46**, 2650.
23 M. J. Dávila and J. Martin Trusler, *J. Chem. Thermodyn.*, 2009, **41**, 35–45.
24 The International Association for the Properties of Water and Steam, Revised Release on the IAPWS Formulation, 1995 for the Thermodynamic Properties of Ordinary Water Substance for General and Scientific Use, 2014, http://www.iapws.org/relguide/IAPWS95-2014.pdf, date of access: 15/01/2015.
25 W. Wagner, *J. Phys. Chem. Ref. Data*, 2002, **31**, 387–535.
26 J. L. F. Abascal and C. Vega, *J. Chem. Phys.*, 2005, **123**, 234505.
27 C. Vega and J. L. F. Abascal, *Phys. Chem. Chem. Phys.*, 2011, **13**, 19663–19688.
28 J. L. F. Abascal and C. Vega, *J. Chem. Phys.*, 2011, **134**, 186101.
29 M. Agarwal, M. P. Alam and C. Chakravarty, *J. Phys. Chem. B*, 2011, **115**, 6935–6945.
30 V. Holten and M. A. Anisimov, *Sci. Rep.*, 2012, **2**, 713.
31 A. Taschin, R. Cucini, P. Bartolini and R. Torre, *Philos. Mag.*, 2011, **91**, 1796–1800.
32 D. Corradini and P. Gallo, *J. Phys. Chem. B*, 2011, **115**, 14161–14166.